THE JOURNAL OF PHYSICAL CHEMISTRY C

Article

pubs.acs.org/JPCC

Morphological, Optical, and Electronic Consequences of Coexisting Crystal Orientations in β-Copper Phthalocyanine Thin Films

Terry McAfee,[†,‡] Benjamin C. Hoffman,[†] Xiao You,[§] Joanna M. Atkin,[∥] Harald Ade,[†] and Daniel B. Dougherty*[,†]

[†]Department of Physics and Organic and Carbon Electronics Laboratory, North Carolina State University, Raleigh, North Carolina 27695, United States

[‡]Department of Physics and Engineering Physics, Tulane University, New Orleans, Louisiana 70118, United States

[§]Department of Applied Physical Science and [∥]Department of Chemistry, University of North Carolina at Chapel Hill, Chapel Hill, North Carolina 27599-3216, United States

ABSTRACT: The crystal structure of the β phase of copper phthalocyanine (CuPc) is a monoclinic herringbone, which is commonly created in thin films by either thermal annealing of α-CuPc at ∼300 °C or deposition on heated substrates. Of the several known CuPc crystal polymorphs, the β phase is of particular interest due to its thermodynamic stability. We observe three coexisting crystal orientations for thin films of β-CuPc to be (101), ($\bar{1}$05), and ($\bar{5}$02) using grazing incidence wide-angle X-ray scattering. Each of the three crystal orientations have distinct surface roughness, as measured by atomic force microscopy, but are electrostatically similar by Kelvin probe force microscopy. However, local optical properties, as measured by micro-UV−vis spectroscopy, are very different in the different domains.

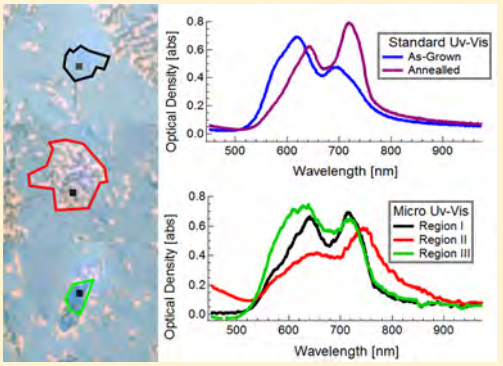

I. INTRODUCTION

The promise of flexible, low cost electronic devices composed of renewable, earth abundant elements has led to increasing research on organic semiconductors over the past ∼20 years. Out of the numerous organic semiconducting materials available, the planar small molecule copper phthalocyanine (CuPc) is not only one of the oldest and most well-studied materials, but to date is still a common choice for organic electronic research due to its chemical stability, high molecular symmetry, facile yet precise film creation capability, and commercial availability. CuPc has been used in the fabrication of nearly all types of organic electronic devices, including diodes,[1] transistors,[2] photovoltaics,[3] light emitting diodes,[4] photodetectors,[5] rectifiers,[6] temperature sensors,[7] radiation dosimeters,[8] and chemical biosensors.[9,10] The growing global demand for cheap energy sources and consumer electronics has brought organic photovoltaics (OPVs) and organic thin film transistors (OTFTs) to the forefront of organic semiconductor research.

The crystal structure and orientation with respect to the substrate of CuPc thin films has been studied by many research groups over the past few decades. The identification and control of crystal formation in organic thin films is quite valuable since the molecular orientation and order is known to have a substantial impact on the performance characteristics of organic electronic devices.[11,12] The choice of substrate, substrate temperature, and film thickness are the primary factors influencing CuPc crystal structure and orientation. The most common crystal polymorphs of CuPc are the α-herringbone,[13] the β-herringbone,[14] and the more recently identified brickstone.[15] In addition to there being several known crystal polymorphs for CuPc thin films, multiple orientations of these crystals have been reported as well. Films grown on substrates below ∼200 °C form either the α-herringbone or brickstone crystals. Films grown on substrates above ∼200 °C, or annealed above ∼300 °C after film growth, form β-herringbone crystals. Additionally, CuPc thin films are known to exhibit coexisting crystal structures and crystal orientations. For example, thickness-dependent morphology transitions from α-herringbone (200) to a brickstone (100) crystal structure on a ZnO(1100)[16] substrate and from brickstone (01$\bar{2}$) to brickstone (11$\bar{2}$) on a graphite substrate[17] have been reported. β-CuPc has been reported to adopt several crystal orientations dependent upon the substrate and fabrication method used, including (010),[18,19] (100),[20−22] (011),[21] ($\bar{1}$01),[23] (302),[21] (20$\bar{1}$),[24−26] (001),[25,26] and (20$\bar{2}$)[25] orientations.

While the (001) and (20$\bar{1}$) orientations are reported commonly in the literature, more often than not, the orientation of β-CuPc crystals in thin film devices is not reported, even though it is known to impact their morphological, optical, and electronic properties. Our work

Received: May 21, 2016
Revised: July 18, 2016
Published: July 28, 2016

DOI: 10.1021/acs.jpcc.6b05043
J. Phys. Chem. C 2016, 120, 18616−18621

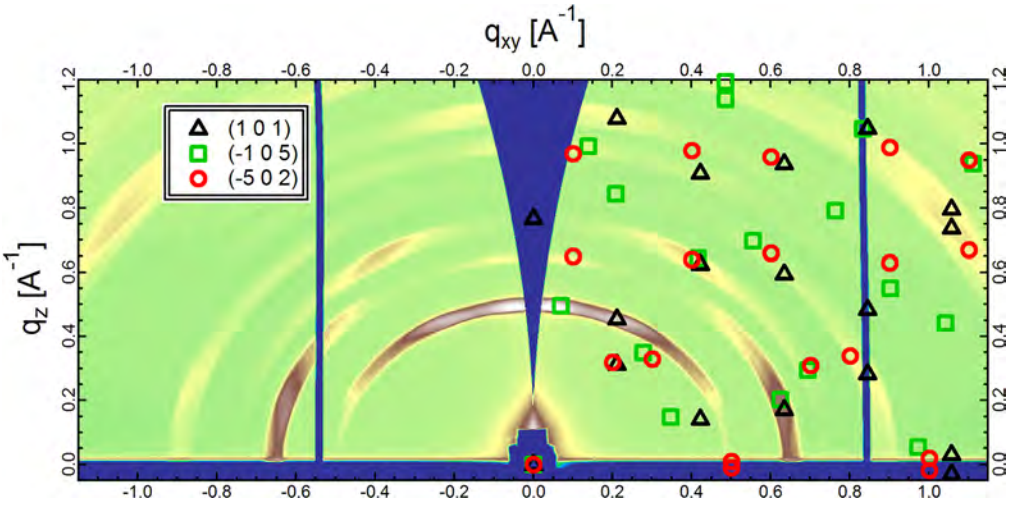

Figure 1. GIWAXS, with forbidden wedge correction, on 100 nm CuPc/glass, annealed at 320 °C for 3 h. Simulated GIWAXS scattering peak locations for (101), ($\bar{1}$05), and ($\bar{5}$02) orientations of β-herringbone CuPc are overplotted.

reported here shows that multiple crystal orientations coexist in β-herringbone CuPc films, leading to spatially inhomogeneous physical properties. This is significant because active layer morphology impacts almost all measures of the performance of organic thin film devices.[27−29] For example, CuPc TFT mobility has been reported to increase from 10^{-5} to 10^{-3} cm^2/V s, for deposition at room temperature or below, to $(1-2) \times 10^{-2}$ cm^2/V s by heating the substrate during deposition.[30] Optimization of the morphology, either by altering the film fabrication procedure or by annealing the fabricated film, is a crucial step in achieving peak performance devices from a given material system. Through a deeper understanding of how to control the thin film morphology, the performance of CuPc based devices could be significantly improved.

We report on the coexistence of three unique β-herringbone domain types present in a 100 nm CuPc film/glass annealed at 320 °C for 3 h. We characterize the morphological, optical, and electronic properties of the three observed domains using grazing incidence wide-angle X-ray scattering (GIWAXS), atomic force microscopy (AFM), Kelvin probe force microscopy (KPFM), and spatially resolved ultraviolet−visible (UV−vis) spectroscopy. The surface morphology was found to vary substantially for each of the three domain types, yet the domains were found to be indistinguishable electrostatically by KPFM. Remarkably, spatially resolved optical absorption shows qualitatively different spectra in the different domains, which we attribute to the effect of local molecular orientation. This multitechnique study emphasizes the complex interplay between crystal structure, nanoscale film morphology, and optical properties that underpins the ongoing development of organic electronic materials.

II. EXPERIMENTAL METHODS

Directly prior to being loaded into the organic molecular beam deposition chamber, glass substrates were cleaned by sonication in acetone and then isopropanol, followed by UV-ozone cleaning, each for 15 min. CuPc (95%) was obtained from Sigma-Aldrich and loaded, as received, into a boron nitride crucible. The crucible was outgassed for ∼24 h in high vacuum prior to film growth. CuPc thin films were grown using thermal evaporation at pressure $<2.0 \times 10^{-6}$ Torr in a high vacuum chamber with a base pressure of 10^{-8} Torr. Deposition rates, monitored using a quartz crystal microbalance, between 0.3 and 0.5 Å/s were used during film growth. Following film growth, samples were annealed at 320 °C for 3 h in a dry nitrogen glovebox with less than 0.1 ppm O_2 and H_2O.

AFM was carried out in ac mode in air using a commercial instrument (Asylum Research MFP-3D). Following each topography line scanned, the same line is scanned again in KPFM mode to measure the surface potential. Commercial AFM tips (Budget Sensors, Tap300E-G) with a nominal radius of ∼10 nm, a nominal resonant frequency of ∼300 kHz, and composed of silicon with a Cr/Pt conductive coating were used.

GIWAXS data was acquired at beamline 7.3.3 at the Advanced Light Source[31] at grazing angles between 0.10 and 0.20° above the plane of the substrate. β-Phase CuPc lattice parameters used for simulation of reciprocal space maps, a = 19.407, b = 4.79, c = 14.628, $\alpha = \gamma = 90°$, and β = 120.933°, as identified by Brown in 1968.[14]

Standard, bulk averaged, ultraviolet−visible (UV−vis) absorption spectroscopy was performed on films before and after annealing using a commercial instrument Cary 50 UV−vis spectrometer. Microscopic UV−vis absorption measurements, with ∼1.2 μm spatial resolution, were performed on individual crystal domains using a commercial microspectrophotometer from CRAIC Technologies Inc. An optical microscope, with a 50× EC Epilpan-Apochromat objective, was used to identify individual crystal domains for the microscopic UV−vis absorption measurements.

III. RESULTS

The crystal structure and orientation is determined using GIWAXS data coupled with simulated reciprocal space maps (RSMs), shown in Figure 1. All of the scattering peaks are smeared circularly about the origin due to the rough surface of the glass substrate. None of the observed scattering peaks were centered along the q_z axis. To identify the structure and orientation of CuPc crystals responsible for the observed GIWAXS scattering peaks, RSMs of α-herringbone, brickstone, and β-herringbone crystal structures with (hkl) orientations for all combinations of h, k, and l between ±8 were considered. All observed scattering peaks were identified to belong to orientations of a β-herringbone crystal structure. Three

DOI: 10.1021/acs.jpcc.6b05043
J. Phys. Chem. C 2016, 120, 18616−18621

different β-herringbone crystal orientations were needed to account for the observed scattering peaks. Out of all of the orientations considered, the (101), ($\bar{1}$05), and ($\bar{5}$02) orientations were found to be in best agreement with the observed scattering peak locations. Importantly, the absence of a scattering peak centered along the q_z axis clearly indicates the absence of the more commonly reported (001) and (20$\bar{1}$) orientations. Figure 2 illustrates the relative angle between the

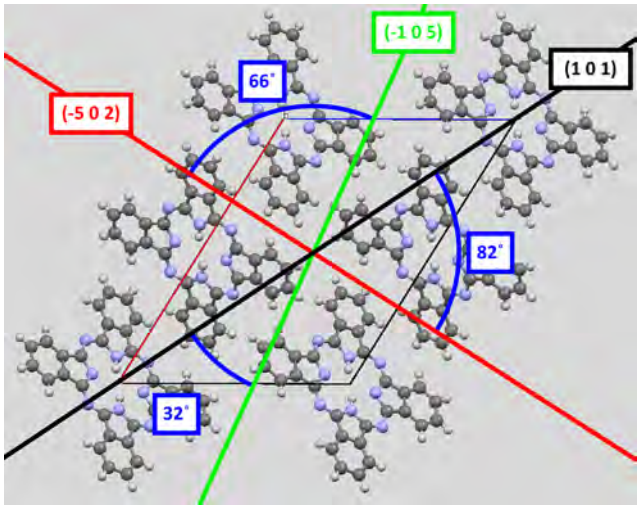

Figure 2. Illustration of molecular arrangement of CuPc molecules in a β-herringbone crystal, as viewed along the *b*-axis. The parallelogram shows the unit cell, with a thin red line and a thin blue line showing the *a*-axis and *c*-axis of the crystal, respectively. The (101), ($\bar{1}$05), and ($\bar{5}$02) crystal planes, and relative angles between these planes, are overplotted.

(101), ($\bar{1}$05), and ($\bar{5}$02) crystal planes, as viewed along the *b*-axis of the β-herringbone crystal. Note that each of these planes is a variation on the "edge-on" molecular orientation with respect to the substrate.

AFM and KPFM were performed to characterize the film morphology and surface potential. Three distinct crystal domain morphologies were observed from the topography, which will be referred to as region I, region II, and region III. Crystal domains from region II are larger in both surface area and height than the two smaller domains, and formed ∼10 μm wide domains exhibiting an average root-mean-square (RMS) surface roughness of 33 ± 4 nm. Crystal domains from regions I and III were observed to be ∼2−5 μm wide, exhibiting average RMS surface roughnesses of 16.7 ± 1.4 nm for region I and 8.3 ± 1.4 nm for region III. The area between region I and region III appears to be a mixture of those two regions.

Identification of the three observed crystal domains for surface roughness and electric potential measurements was performed by manually masking the topography data based on the unique characteristics of each crystal, as shown in Figure 3a for one of the scans. Figure 3b shows the KPFM surface potential for the topography shown in Figure 3a. Using the same masks, identified from the topography, the average surface potential was calculated for each of the three observed domain types. The average surface potential statistics for six scans, taken at three different macroscopic locations on the sample, are shown in Figure 3c. Remarkably, there was no measurable difference in the surface potential for the three domain types. The *b*-axis for all three orientations is aligned parallel to the substrate, meaning the surface potential variation is due solely to the cross-cut of the *a*-axis and *c*-axis of the crystal. Since the *a*-axis and *c*-axis of the crystal are physically similar, it is not surprising that their surface potentials are indistinguishable by KPFM.

Standard UV−vis absorption spectroscopy was performed on the as-grown sample and again after annealing. As expected, the UV−vis absorption spectra for the as-grown, α-phase, film and the postannealed, β-phase, film agree with previous reports in

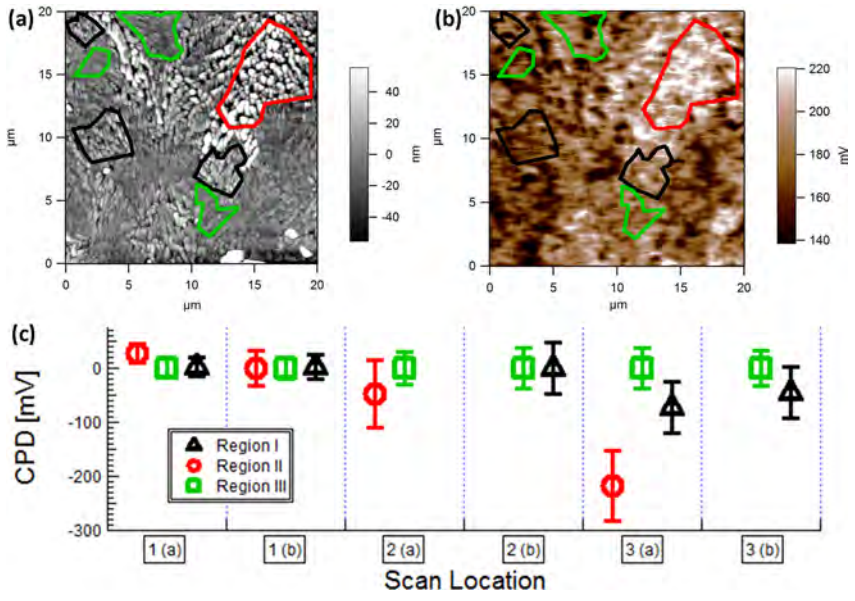

Figure 3. AFM data, shown in (a), collected simultaneously with KPFM, shown in (b), on 100 nm CuPc/glass, annealed at 320 °C for 3 h. In agreement with the GIWAXS data, three distinct topographies are identified from the AFM. The average surface potential for these domains is shown in (c), indicating no measurable difference between the three crystal orientations. Two scans within a 90 μm area are shown for three different macroscopic locations on the sample, which were several millimeters apart. To account for variations in the surface potential of different AFM tips, the CPD from each scan is offset to make the average surface potential of region II zero.

DOI: 10.1021/acs.jpcc.6b05043
J. Phys. Chem. C 2016, 120, 18616−18621

the literature.[32−34] While the as-grown films were featureless in the visual light microscope, the annealed film formed visible domains, as shown in Figure 4a. Since the absorption profile of a material depends not only on the crystal phase, but on the orientation of the crystal as well, micro-UV−vis spectroscopy was employed on individual domains.

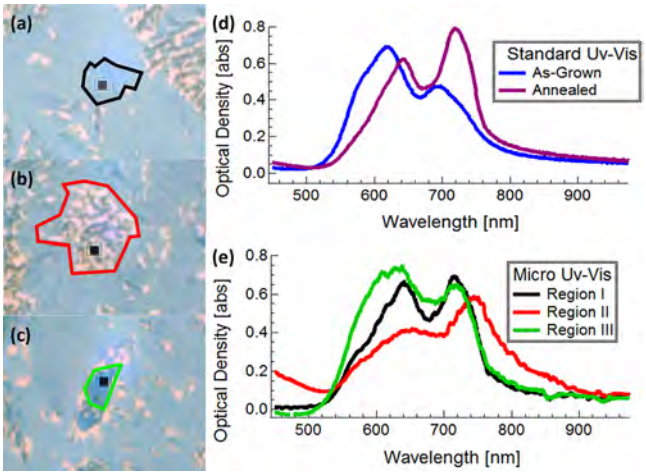

Figure 4. Visual light microscope on 100 nm CuPc/glass, annealed at 320 °C for 3 h, with the black square indicating the location the micro-UV−vis spectra were collected for (a) region I, (b) region II, and (c) region III. Standard, bulk averaged UV−visible spectroscopy of as-grown and annealed films shown in (d). Micro-UV−visible spectroscopy shown in (e), collected at locations indicated in (a), (b), and (c).

The absorption spectra were found to vary significantly depending on which domain type was measured, as shown in Figure 4e. For comparison, the standard, bulk averaged, UV−vis absorption spectrum is also plotted in Figure 3d. As-grown CuPc has peaks at 620 and 693 nm which are red-shifted upon annealing to 642 and 719 nm. Region I has peaks at 641 and 715 nm. Region II has broad peaks at 650 and 745 nm. Region III has peaks at 632 and 718 nm.

The absorption peak at 745 nm in region II is of particular interest since it absorbs at a higher wavelength than observed by either film in the bulk averaged UV−vis absorption spectra. An OPV made from equal amounts of crystals from region II and region III would have an absorption range from ∼550 to 800 nm, which is an ∼25% larger absorption range than that of either of the bulk average films, and would have a significantly more uniform absorption profile.

IV. DISCUSSION

Despite the coexistence of three different β-herringbone crystal orientations, each with significantly different absorption spectra, the average absorption spectrum agreed with the literature. This indicates that the coexistence of multiple orientations may be quite common for β-CuPc films. A recent publication using inert gas flow temperature gradient physical vapor deposition reported the growth of three distinct microscopic β-CuPc crystal shapes, each with distinct UV−vis absorption spectra, dependent on the formation temperature, illustrating the diversity possible in crystal growth even under fixed macroscopic conditions.[35] Our observations here are a further manifestation of the complexities of organic molecular solid formation wherein multiple orientations of a fixed crystal structure with respect to the substrate are close enough in energy to coexist in a film.

Interestingly, the (101), ($\bar{1}$05), and ($\bar{5}$02) crystal orientations observed in our films have their b-axis aligned parallel to the substrate, yet are very different cross sections of the a-axis and c-axis of the crystal, as shown in Figure 2. Figures 3 and 4 clearly demonstrate that each crystal orientation exhibits significantly different morphological properties, which is known to influence charge transport and optical excitation. The variation in morphology between each domain type as well as the large RMS roughness exhibited by the β-CuPc film may be detrimental for organic electronics applications. The abundance of grain boundaries in the film, in particular, might inhibit charge transport in the plane of the film, making it less suitable for TFT applications. In contrast, the large surface roughness exhibited in domains from region I and region II could provide better exciton dissociation if employed in a bilayer OPV due to increased interfacial area between the donor and acceptor materials.

Given that at least eight different orientations of β-herringbone CuPc have been reported in the literature, none of which were present in our films, it seems pertinent to discuss the ease of misidentification of crystal orientation by X-ray diffraction (XRD). The ($\bar{1}$05) and ($\bar{5}$02) orientations observed in our films do not have a scattering peak on the q_z axis (q_{xy} = 0), meaning that these orientations would not result in a diffraction peak in standard XRD if the crystals are well-ordered on a flat substrate. Orientation disorder resulting from crystals formed on a rough substrate, such as glass and ITO, results in peaks near q_{xy} = 0 to broaden enough to include scattering along the q_z axis. As such, scattering peaks observed in a standard θ−2θ XRD may detect peaks on the q_z axis that are actually broadened tails of scattering peaks located off the q_z axis. For example, the [001] reflection at q_{xy} = 0.070 Å^{-1}, q_z = 0.496 Å^{-1} of a ($\bar{1}$05) oriented crystal could be easily mistaken for the [001] reflection of a (001) oriented crystal, which has a diffraction peak at q_{xy} = 0 Å^{-1}, q_z = 0.50 Å^{-1}. Similarly, the [201] reflection of a ($\bar{5}$02) oriented crystal, at q_{xy} = 0.095 Å^{-1}, q_z = 0.650 Å^{-1}, could be mistaken for the [201] reflection of a (20$\bar{1}$) oriented crystal, which has a diffraction peak at q_{xy} = 0 Å^{-1}, q_z = 0.66 Å^{-1}. Thus, the correct identification of β-herringbone crystal orientation in thin films may be difficult by the θ−2θ mode of XRD alone, especially for films grown on rough substrates. The asymmetric charge mobility and optical absorption properties of β-CuPc suggest that a device with uniformly oriented (101), ($\bar{1}$05), or ($\bar{5}$02) crystallites would each have very different optical and electrical properties.

The spatially inhomogeneous optical absorption in the three different domains is very important to consider. In CuPc, the region between 500 and 800 nm is called the Q-band. It arises from π−π* optical transitions and has a characteristic double peak shape that originates from the breaking of the LUMO degeneracy when molecules are slightly distorted in the crystal packing structure.[36] The relative intensity of each excitation in the Q-band is related to the alignment of incoming light polarization with the associated transition dipole moments of the molecule. Thus, it is expected that the different crystal orientations will give rise to different relative intensities within the Q-band.

Nevertheless, such a micrometer-scale inhomogeneity in optical absorption properties has rarely been considered in optoelectronic device analysis. The significant spatial nonuniformity observed here shows clear room for improvement

DOI: 10.1021/acs.jpcc.6b05043
J. Phys. Chem. C 2016, 120, 18616−18621

toward single crystal benchmarks. The large RMS roughness is indicative of three-dimensional growth of separate crystallites within a domain, which is particularly evident in the "big rough" domains, resulting in excessive grain boundaries that might be expected to lead to poor charge mobility parallel to the substrate. While charge mobility parallel to the substrate is important for TFT applications, it is the charge mobility perpendicular to the substrate that is most influential for OPV device performance. Thus, a donor layer composed of a mixture of region II and region III has the potential for achieving a high performance bilayer OPV device. The complementary absorption spectrum provides nearly uniform absorption across from 550 to 800 nm, which is a much broader absorption spectrum than what has yet been experimentally achieved over macroscopic areas. Additionally, the large roughness exhibited by region II would induce a large interfacial area with the acceptor material, which should increase exciton dissociation efficiency. It implies that morphology influences not only the details of exciton and carrier transport and lifetime but also exciton creation.

V. SUMMARY AND CONCLUSIONS

In this paper, we report on the coexistence of three distinct crystal domain types present in a 100 nm CuPc/glass film annealed at 320 °C for 3 h. Using GIWAXS, we determined the three crystal domains to be (101), ($\bar{1}$05), or ($\bar{5}$02) orientations of the β-herringbone crystal structure, which to our knowledge have not been previously reported for any β-CuPc thin film. AFM and UV−vis absorption measurements performed on individual crystal domains reveal each of the three crystal domain types have very different morphological and optical absorption properties, yet the electrical surface potential is indistinguishable by KPFM.

Since the crystal structure and orientation are known to have a significant impact on the performance of organic electronic devices, the identification and manipulation of crystal species within the active layer of devices is very beneficial. We assert that standard $\theta-2\theta$ XRD is not sufficient for determination of β-CuPc crystal orientation. It may be beneficial to revisit previous β-CuPc thin film device studies where standard $\theta-2\theta$ XRD was used to determine the crystal orientation, especially in cases where ($\bar{2}$01) or (001) orientations were reported for films grown on rough substrates such as ITO. Importantly, our work shows that crystal orientation is decisive in determining the optical absorption and that this can show very significant spatial variations when crystal orientations coexist. Thus, it is crucial to correctly identify orientations to understand and control functional properties.

Overall, the coexistence of three different crystal domain types within the β-CuPc film is probably detrimental for organic electronic applications. The abundance of grain boundaries between domain types, as well as within the two rougher domain types, in particular, would decrease in-plane charge mobility. By further investigation of the temperature dependence of β-CuPc film growth morphology, it may be possible to achieve thin films of uniformly oriented crystallites. More importantly, this well-studied system is a valuable case study illustrating morphological complexity and its functional impacts, even in films with nominally understood crystal structures.

AUTHOR INFORMATION

Notes

The authors declare no competing financial interest.

ACKNOWLEDGMENTS

This work was supported by the U.S. Department of Energy (DE-FG02-98ER45737) for GIWAXS characterization and NSF CAREER Award DMR-1056861 for AFM and KPFM characterization and growth. The Advanced Light Source is supported by the Director, Office of Science, Office of Basic Energy Sciences, of the U.S. Department of Energy under Contract No. DE-AC02-05CH11231. Special thanks to beamline 7.3.3 Staff Alexander Hexemer and Eric Schaible for help with data acquisition and maintenance. T.M. was partially supported by GAANN Fellowships. Micro-UV−visible absorption measurements were performed at Chapel Hill Analytical and Nanofabrication Laboratory (CHANL), which is partially supported by the NSF NNCI program (Award No. 1542015).

REFERENCES

(1) Gould, R. D.; Hassan, A. K. *Thin Solid Films* **1990**, *193−194*, 895.
(2) Yuan, J. F.; Zhang, J.; Wang, J.; Yan, X. J.; Yan, D. H.; Xu, W. *Appl. Phys. Lett.* **2003**, *82*, 3967.
(3) Antohe, S.; Tugulea, L. *Physica Status Solidi a-Applied Research* **1991**, *128*, 253.
(4) Lee, S. T.; Wang, Y. M.; Hou, X. Y.; Tang, C. W. *Appl. Phys. Lett.* **1999**, *74*, 670.
(5) Farooq, A.; Karimov, K. S.; Ahmed, N.; Ali, T.; Alamgir, M. K.; Usman, M. *Phys. B* **2015**, *457*, 17.
(6) Chowdhury, A.; Biswas, B.; Sanyal, M. K.; Mallik, B. *Sci. Adv. Mater.* **2013**, *5*, 1857.
(7) Farooq, A.; Karimov, K. S.; Wahab, F.; Ali, T.; Abbas, S. Z. *J. Optoelectron. Adv. Mater.* **2015**, *17*, 822.
(8) Arshak, K.; Arshak, A.; Zleetni, S.; Korostynska, O. *IEEE Trans. Nucl. Sci.* **2004**, *51*, 2250.
(9) Li, M. T.; Yang, R. S.; Yu, L. Y. In *Functional Materials and Nanotechnology*; Xu, B., Li, H. Y., Eds.; Trans Tech Publications Ltd.: Stafa-Zurich, 2012; Vol. *496*, p 439.
(10) Mensing, J. P.; Kerdcharoen, T.; Sriprachuabwong, C.; Wisitsoraat, A.; Phokharatkul, D.; Lomas, T.; Tuantranont, A. *J. Mater. Chem.* **2012**, *22*, 17094.
(11) Ostrick, J. R.; Dodabalapur, A.; Torsi, L.; Lovinger, A. J.; Kwock, E. W.; Miller, T. M.; Galvin, M.; Berggren, M.; Katz, H. E. *J. Appl. Phys.* **1997**, *81*, 6804.
(12) Chowdhury, A.; Biswas, B.; Mallik, B. *Sci. Adv. Mater.* **2013**, *5*, 1297.
(13) Ashida, M.; Uyeda, N.; Suito, E. *Bull. Chem. Soc. Jpn.* **1966**, *39*, 2616.
(14) Brown, C. J. *J. Chem. Soc. A* **1968**, 2488.
(15) Hoshino, A.; Takenaka, Y.; Miyaji, H. *Acta Crystallogr., Sect. B: Struct. Sci.* **2003**, *59*, 393.
(16) Cruickshank, A. C.; Dotzler, C. J.; Din, S.; Heutz, S.; Toney, M. F.; Ryan, M. P. *J. Am. Chem. Soc.* **2012**, *134*, 14302.
(17) McAfee, T.; Gann, E.; Guan, T. S.; Stuart, S. C.; Rowe, J.; Dougherty, D. B.; Ade, H. *Cryst. Growth Des.* **2014**, *14*, 4394.
(18) Xiao, Y.; Li, Y.; Zhang, M.; Wang, F. X.; Pan, G. B. *Chem. Lett.* **2011**, *40*, 544.
(19) Xiao, K.; Li, R. J.; Tao, J.; Payzant, E. A.; Ivanov, I. N.; Puretzky, A. A.; Hu, W. P.; Geohegan, D. B. *Adv. Funct. Mater.* **2009**, *19*, 3776.
(20) Padma, N.; Sawant, S. N.; Sen, S.; Gupta, S. K. In *Solid State Physics: Proceedings of the 57th DAE Solid State Physics Symposium 2012*; Chauhan, A. K., Murli, C., Gadkari, S. C., Eds.; AIP Conference Proceedings 1512; American Institute of Physics: Melville, NY, 2013; p 786.
(21) Berger, O.; Fischer, W. J.; Adolphi, B.; Tierbach, S.; Melev, V.; Schreiber, J. *J. Mater. Sci.: Mater. Electron.* **2000**, *11*, 331.

DOI: 10.1021/acs.jpcc.6b05043
J. Phys. Chem. C 2016, 120, 18616−18621

(22) Chintakula, G.; Rajaputra, S.; Singh, V. P. *Sol. Energy Mater. Sol. Cells* **2010**, *94*, 34.
(23) Jung, J. S.; Lee, J. W.; Kim, K.; Cho, M. Y.; Jo, S. G.; Joo, J. *Chem. Mater.* **2010**, *22*, 2219.
(24) Hassan, A. K.; Gould, R. D. *Physica Status Solidi a-Applied Research* **1992**, *132*, 91.
(25) Wang, C. Y.; Cho, C. P.; Perng, T. P. *Thin Solid Films* **2010**, *518*, 6720.
(26) Basova, T. V.; Kol'tsov, E. K.; Igumenov, I. K. *Sens. Actuators, B* **2005**, *105*, 259.
(27) Liu, S. H.; Wang, W. C. M.; Briseno, A. L.; Mannsfeld, S. C. E.; Bao, Z. N. *Adv. Mater.* **2009**, *21*, 1217.
(28) Yang, J. L.; Yan, D. H. *Chem. Soc. Rev.* **2009**, *38*, 2634.
(29) Vakhshouri, K.; Kesava, S. V.; Kozub, D. R.; Gomez, E. D. *Mater. Lett.* **2013**, *90*, 97.
(30) Bao, Z.; Lovinger, A. J.; Dodabalapur, A. *Appl. Phys. Lett.* **1996**, *69*, 3066.
(31) Hexemer, A.; Bras, W.; Glossinger, J.; Schaible, E.; Gann, E.; Kirian, R.; MacDowell, A.; Church, M.; Rude, B.; Padmore, H. In *XIV International Conference on Small-Angle Scattering*; Ungar, G., Ed.; Journal of Physics Conference Series 247; IOP Publishing: Bristol, U.K., 2010.
(32) Farag, A. A. M. *Opt. Laser Technol.* **2007**, *39*, 728.
(33) Karan, S.; Mallik, B. *Solid State Commun.* **2007**, *143*, 289.
(34) E, J. Y.; Kim, S.; Lim, E. J.; Lee, K. J.; Cha, D. J.; Friedman, B. *Appl. Surf. Sci.* **2003**, *205*, 274.
(35) Liu, F. M.; Sun, J.; Xiao, S.; Huang, W. L.; Tao, S. H.; Zhang, Y.; Gao, Y. L.; Yang, J. L. *Nanotechnology* **2015**, *26*, 225601.
(36) Iyechika, Y.; Yakushi, K.; Kuroda, H. *Chem. Phys.* **1984**, *87*, 101.

DOI: 10.1021/acs.jpcc.6b05043
J. Phys. Chem. C 2016, 120, 18616−18621